Korean J. Chem. Eng., 32(6), 1178-1187 (2015)
DOI: 10.1007/s11814-014-0315-9

pISSN: 0256-1115
eISSN: 1975-7220

The role of tetragonal-metal-organic framework-5 loadings with extra ZnO molecule on the gas separation performance of mixed matrix membrane

Mehrzad Arjmandi*,†, Majid Pakizeh*,†, and Omid Pirouzram**

*Department of Chemical Engineering, Faculty of Engineering, Ferdowsi University of Mashhad, Mashhad, Iran
**Department of Chemical Engineering, Faculty of Engineering, Kurdistan University, Kurdistan, Iran
(*Received 20 August 2014 • accepted 20 October 2014*)

Abstract−The effect of more ZnO molecule in tetragonal structure of MOF-5 than cubic structure on the gas permeation properties of T-MOF-5/polyetherimide mixed matrix membranes was investigated. T-MOF-5 was first successfully synthesized and carefully characterized by XRD, FTIR, SEM and N_2 adsorption technique at 77 K. Novel T-MOF-5/PEI MMMs were prepared using solution casting method and characterized by FTIR and SEM. The SEM pictures of the MMMs showed that T-MOF-5 nanocrystals changed the morphology of PEI and exhibited acceptable contacts between the filler particles and the polymer chains. Gas permeation properties of these membranes with different T-MOF-5 contents were studied for pure H_2, CO_2, CH_4 and N_2 gases. Permeation measurement showed that the all gases' permeability, diffusivity and solubility were increased with T-MOF-5 loading. H_2 permeability and the ideal selectivity of H_2/CO_2 and H_2/CH_4 in MMM with 25 wt% loading of T-MOF-5 nanocrystals were increased. This behavior was attributed to more ZnO molecule in T-MOF-5 structure. The experimental gas permeations through T-MOF-5/PEI nanocomposite with different filler loadings were fitted on Higuchi model. Good agreement between the experimental data and the predicted gas permeability was obtained.

Keywords: Mixed Matrix Membrane, Metal Organic Framework, Tetragonal-MOF-5, Zn, Gas Separation

INTRODUCTION

Novel membrane technologies can potentially present economic, environmental, and high performance interests to virtually any process associated with gas separation [1]. Polymer membranes incur lower production costs and can be easily developed to hollow fiber modules or spiral wound, but they have lower permeability and selectivity than inorganic membranes for gas separations [2,3]. To improve polymeric membrane performance, considerable research has focused on the addition of inorganic materials such as zeolites or activated carbon sieves to polymers [4-11]. These so-called mixed matrix membranes (MMMs) combine useful molecular sieving properties of inorganic molecular sieves with the favorable mechanical and processing properties of polymers [4-8]. One of the recent developments in relation to the membrane fillers is the use of new materials, known as metal-organic frameworks (MOFs), as potential fillers in the polymer matrix [2,12-15]. Metal organic frameworks, consisting of organic linkers and inorganic joints, are relatively new materials with novel structural and promising sorption properties [16]. Thus, these novel porous adsorbents have been intensively studied as promising nanoporous materials that may have a tremendous impact in fields such as gas or liquid separations, catalysis, chemical sensing, gas storage, ion exchange and polymerization [17-20].

Among the articles reporting new types of MOF materials, the $Zn_4O_{13}C_{24}H_{12}$ framework known as MOF-5 or IRMOF-1 is the most well studied MOFs with promising industrialization potential [2]. MOF-5 consisted of Zn_4O as metal clusters connected by 1, 4-benzenedicaboxylate (BDC) as a linear linkers to form a porous cubic $Zn_4O(BDC)_3$ framework [21].

Zhang and Hu [22] reported that there are two types of porous crystalline MOF-5: the cubic structure [23] (C-MOF-5) and tetragonal structure [24] (T-MOF-5). They indicated that the composition of T-MOF-5 and C-MOF-5 samples was calculated with the formula of composition $Zn_4O_{13}C_{24}H_{12.6}(ZnO)_{1.59}(H_2O)_{1.74}$ and $Zn_{4.28}O_{12.8}C_{24}H_{11.3}$, respectively. According to the stoichiometric formula of novel MOF-5 ($Zn_4O_{13}C_{24}H_{12}$) the formula of C-MOF-5 sample is consistent with the novel MOF-5. In contrast, the formula composition of T-MOF-5 sample is very different from the novel MOF-5, because ZnO and H_2O were present.

Arjmandi and Pakizeh [25] reported that the T-MOF-5 had lower surface area, lower porosity, smaller and more uniform pore size, and more ZnO molecules than C-MOF-5 (pore size 8.67 Å). The differences between the two nanocrystals structure bring about the different behavior in MMMs as filler.

Sarmiento-Perez et al. [26] used the grand canonical Monte Carlo (GCMC) simulation of CO_2 adsorption in MOF-5 and found a surprising role of the BDC organic ligand in this process. They reported that the organic ligands (BDC) have an important role in the CO_2 adsorption on MOF-5, and, when considered in isolation, adsorption to sites near the ligand is only slightly less favorable than at Zn_4O oxoclusters.

Spencer et al. [27] used neutron powder diffraction to determine the H_2 adsorption sites in MOF-5 structure. The results show that

†To whom correspondence should be addressed.
E-mail: Mehrzad.Arjmandi89@gmail.com, Pakizeh@um.ac.ir

the metal-oxide cluster (ZnO) is primarily responsible for the adsorption, while the organic ligand (BDC) plays only a secondary role. These results hold the key to optimizing MOF-5 for H_2 storage applications.

Skoulidas and Sholl [28] applied the equilibrium molecular dynamics (MD) and GCMC to calculate the diffusion and adsorption of a number of small gas species (such as CH_4, CO_2, N_2, and H_2) in C-MOF-5. They reported that in low pressure (1-2 bar) for CH_4, CO_2, N_2, and H_2 no significant increase in gas adsorption and in high pressure (6-7 bar) only CO_2 adsorption was increased. They also showed that the diffusion of H_2 is much higher than CH_4, CO_2 and N_2.

In our previous work [29], we reported the synthesis and characterization of C-MOF-5/PEI MMMs to study the effect of C-MOF-5 on the CH_4, CO_2, N_2, and H_2 gas permeation through the C-MOF-5/PEI MMMs. The results showed that the C-MOF-5 nanocrystals facilitated the gas transport along the membranes, and for all gases the permeabilities, diffusivities and solubilities of the MMMs increased with increasing loading of C-MOF-5 nanocrystals at ambient temperature and pressure of 6 bar. The rate of increase of CO_2 solubility was higher than the CH_4 solubility for all prepared C-MOF-5/PEI MMMs. For low percentage of C-MOF-5, the H_2/CO_2, H_2/CH_4, and CO_2/CH_4 permselectivity was more than the pure PEI membrane. By increase of C-MOF-5 loading, the value of H_2/CO_2 permselectivity was decreased as a result of the increased CO_2 solubility in C-MOF-5 pores.

In the present work, we synthesized and incorporated of T-MOF-5 nanocrystals into a polyetherimide (PEI) matrix. The aim was therefore to study the effect of more ZnO in the structure of T-MOF-5 on performance of the T-MOF-5/PEI MMMs as well as to compare the resulting membranes with C-MOF-5 MMMs made with the same PEI matrix. Prepared T-MOF-5 and MMMs were characterized by using powder X-ray diffraction (XRD), Fourier-transform infrared spectroscopy (FTIR), scanning electron microscopy (SEM), N_2 adsorption technique and single gas permeation.

EXPERIMENTAL

1. Materials

Zinc nitrate hexahydrate ($Zn(NO_3)_2{\cdot}6H_2O$, >99%), 4-dicarboxylic acid (BDA, >99%), Benzene-1, N,N-dimethylformamide (DMF, 99.8%, H_2O <0.15%), N-Methyl-2-Pyrrolidone (NMP), Triethylamine (TEA) and Hydrogen peroxide (H_2O_2) were used without further treatment and obtained from Sigma-Aldrich. HPLC grade water was used as received and acquired from Fisher. Zinc nitrate hexahydrate ($Zn(NO_3)_2{\cdot}6H_2O$, 98%) was stored under nitrogen atmosphere to reduce exposure to moisture. Polyetherimide (PEI) with average molecular weight of 30,000 kg/kmol was purchased from Sigma-Aldrich. H_2, CO_2, CH_4 and N_2 gas cylinders were obtained from Air Liquid for the permeation experiments. For CO_2 the purity of the gas was greater than 99.5% and for H_2, CH_4 and N_2 was greater than 99.99%.

2. Synthesis of T-MOF-5 Nanocrystals

T-MOF-5 nanocrystals were synthesized via the approaches developed by Kaye et al. [24]. $Zn(NO_3)_2{\cdot}6H_2O$ (1.19 g) and H_2BDC (0.34 g) were dissolved in a solution containing 40 ml DMF in a 100 ml Pyrex bottle during stirring at room temperature. Then, three drops of H_2O_2 aqueous solution was added to the bottle. Thereafter, triethylamine (TEA) (2.3 ml) was slowly added dropwise into the Pyrex bottle under strong agitation and temperature of 70 °C for 2 h. Then the reaction vessel was placed in an oven at 100 °C for 15 h. The reaction vessel was removed from the oven and allowed to cool to room temperature. After decanting of DMF, the remaining white solid was washed and filtered with DMF three times. Finally, the sample was dried at 125 °C and held at this temperature for 1 day under vacuum conditions.

3. Fabrication of Pure PEI Membrane and T-MOF-5/PEI MMM

To obtain the pure PEI membrane solution, 1 g of the PEI was dissolved in 4 g NMP and stirred for 30 h in 60 °C. To prepare the T-MOF-5/PEI MMMs solution, 0.05 g (5% loading), 0.15 g (15%) and 0.25 g (25%) of T-MOF-5 powder were added to of 3.6 g NMP and stirred in an ultrasonic water bath for 5 min. After priming of the T-MOF-5 particles [7,16,30] by adding 0.5 g of polymer solution to the T-MOF-5 suspension, 0.85 g (for loading 5%), 0.75 g (15%) and 0.65 g (25%) of PEI were added to solution under extreme mobility for 1 d. After the pure PEI membrane solution and the T-MOF-5/PEI MMMs solution were placed in two glass vessels overnight, uniform films were cast using a casting bar with thicknesses of 30 to 40 μm on a smooth glass plate. The glass plate was placed in a vacuum oven at 70 °C and low pressure for 2 d to evaporate the residual solvents completely. After the glass plate was removed by placing it in a water bath, the thickness of the manufactured membrane was measured with a digital micrometer at various locations. The typical membrane area located at test cell was 9.62 cm^2.

4. Characterization of T-MOF-5, PEI and MMMs

X-ray diffraction data for T-MOF-5 was obtained by using a Philips Analytical X-pert powder diffractometer (PW3710 model) system with Cu Ka radiation (λ=1.54056 Å). FTIR spectra of the T-MOF-5 and MMMs were recorded at room temperature on a Thermo Nicolet Avatar 370. N_2 adsorption isotherms were measured at 77 K on a Belsorp mini II analyzer using standard continuous procedures. Surface area was determined by BET [31] method. Pore size distribution of T-MOF-5 was evaluated using the SHN1 method [32]. SEM images of T-MOF-5 and MMMs were taken on a Cam Scan SEM model KYKYEM3200 microscope.

5. Gas Permeability, Solubility and Diffusivity Measurements

Single-gas permeabilities were measured for H_2, CO_2, CH_4 and N_2 using a variable-volume/constant-pressure experimental method at 25 °C and pressure of 6 bar [33,34]. A schematic of experimental set-up is presented in our previous work [29].

According to the known pressure difference across the membrane, membrane thickness and effective membrane surface, the gas permeability of membranes (p_i) and the ideal selectivity of penetrant i to penetrant j ($\alpha^p_{i,j}$) were calculated by using the following equations:

$$P_i = \frac{l}{A\Delta P} \times \frac{dV_i}{dt} \tag{1}$$

$$\alpha^p_{i,j} = \frac{p_i}{p_j} \tag{2}$$

where P_i (P_j) represents the gas permeability of penetrant i (j) (Bar-

rer), ΔP is the transmembrane pressure drop (cmHg), A is the effective membrane area (cm^2), l is the membrane thickness (cm) and dV_i/dt is the permeation rate (cm^3(STP)/s).

The diffusion coefficient (D) was determined by the time lag method, represented by Eq. (3):

$$D = \frac{l^2}{6\theta} \quad (3)$$

where the time-lag θ is simply the time-intercept of a linear fit of the steady-state permeate and l is the membrane thickness. The solubility coefficient (S) was then calculated as:

$$S = \frac{P}{D} \quad (4)$$

For the calculation of diffusivities of the slow diffusing gases, the time-lag method can be reliably used [35,36] and for H_2, due to the short time lag of this gas, the solubility and diffusivity cannot be calculated reliably with this method [3].

RESULTS AND DISCUSSION

1. T-MOF-5 Nanocrystals

T-MOF-5 was characterized by a variety of different techniques. The crystal structure and phase purity was first characterized by the X-ray diffraction (XRD) pattern. Fig. 1 shows the powder XRD pattern of the T-MOF-5. The XRD pattern of T-MOF-5 is consistent with those reported in the literature [22]. Theoretically, the highlight characteristic of T-MOF-5 can be examined from four distinctive reflections at 2θ equal to 6.9°, 9.9°, 13.7° and 15.3° which correspond to reflection sites (2 0 0), (2 2 0), (4 0 0) and (4 2 0), respectively [22,23]. The most remarkable difference between the XRD patterns of T-MOF-5 and C-MOF-5 is the relative intensities of the (2 0 0) reflection and (2 2 0) reflection [22,23]. The intensity of (2 0 0) reflection was much higher than that of (2 2 0) reflection for C-MOF-5 [22,37]. In contrast, if the structure of MOF-5 changed from the cubic to the tetragonal, the intensity of (2 0 0) reflection became smaller than that of (2 2 0) reflection (Fig. 1) [21,22]. Very sharp peaks below 10° (with 2θ of 6.9 and 9.9) were observed on the XRD patterns of the tetragonal and the cubic MOF-5s, indicating that both laboratory-prepared MOF-5s have highly crystalline structure.

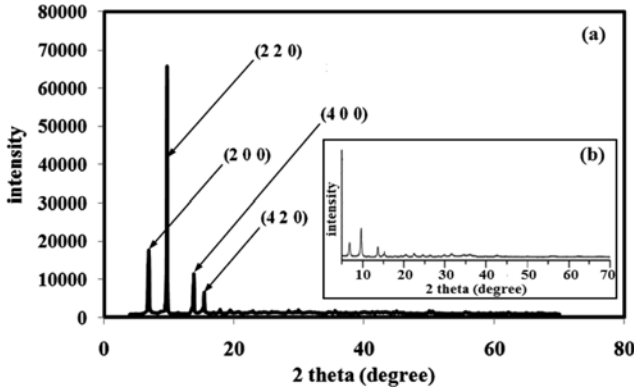

Fig. 1. XRD pattern of T-MOF-5 for (a) this study and (b) Ref. [22].

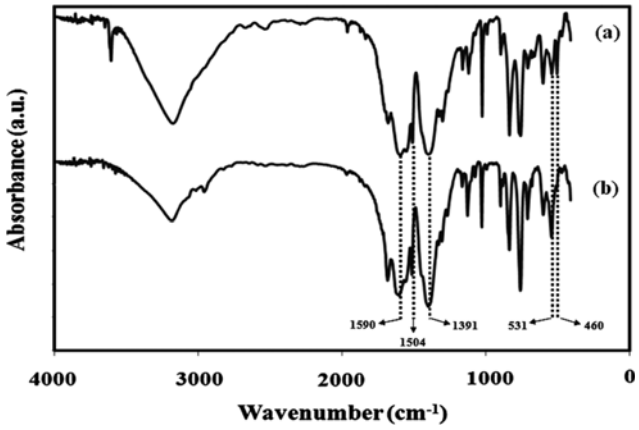

Fig. 2. FTIR spectra of (a) T-MOF-5 and (b) C-MOF-5 [29].

Fig. 2 shows the FT-IR spectra of the T-MOF-5 compared to C-MOF-5 [29], over the wave-number range 4,000-400 cm^{-1}. The presence of two peaks at 1,590 and 1,504 cm^{-1} and one peak at 1,391 cm^{-1} corresponds to the symmetric and asymmetric stretching of COO groups in carboxylic, respectively [38,39]. The vibration bands at 700-1,200 cm^{-1} can be attributed to the terephthalate compounds [38]. The bands around 400-530 cm^{-1} are attributed to ZnO molecule [38,40]. According to results it can be demonstrated that the most remarkable difference between the FT-IR spectra of T-MOF-5 and C-MOF-5 is in the bands around 400-530 cm^{-1}. The T-MOF-5 has an additional peak in the range of 400-530 cm^{-1} than C-MOF-5. The broad bands at 2,800-3,600 cm^{-1} are indicative of the presence of hydroxyl groups (OH) in the metal coordination sphere [38]. According to results, the difference between the FT-IR spectra of T-MOF-5 and C-MOF-5 around 400-530 cm^{-1} is attributed to the presence of ZnO species extra phase in the pores [22]. This is consistent with the elemental analysis results reported by Zhang and Hu [22].

The formation of extra ZnO molecule in T-MOF-5 than C-MOF-5 is due to the reaction between zinc nitrate and H_2O_2 during the synthesis of T-MOF-5. For synthesis of the T-MOF-5 nanocrystal the TEA and H_2O_2 were added into DMF solution of zinc nitrate

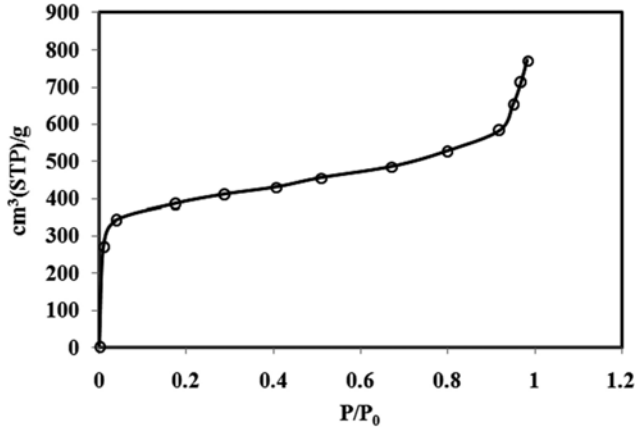

Fig. 3. N_2 adsorption isotherm of T-MOF-5 at 77 K.

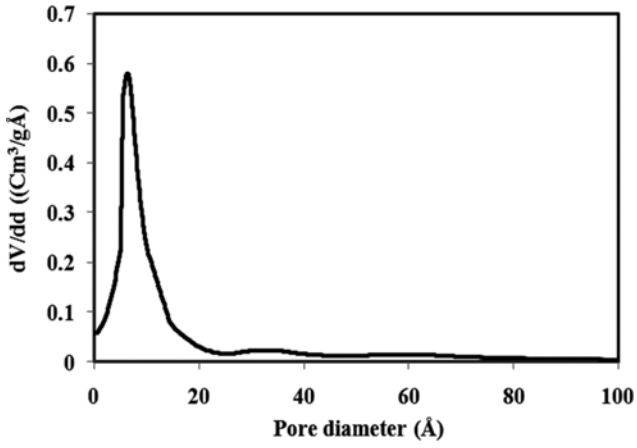

Fig. 4. Pore size distribution of T-MOF-5.

Table 1. Pore textural property of T-MOF-5

Species	BET specific surface area (m^2/g)	Pore diameter (Å)	Pore volume (cm^3/g)
T-MOF-5	1280	6.30	0.59

and H_2BDC. TEA was used for the deprotonation of H_2BDC and its reaction with Zn^{2+} ions [22]. Also H_2O_2 acted as an oxygen precursor to progress the reaction of H_2BDC and zinc nitrate to form MOF-5 nanocrystal structure [22]. However, H_2O_2 can also result

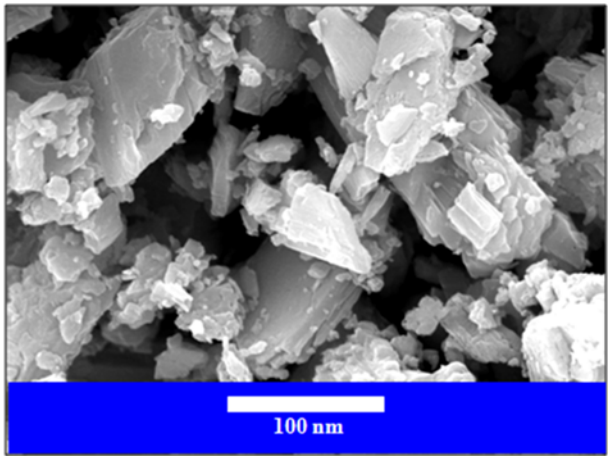

Fig. 5. SEM image of T-MOF-5; 90 nm particle size.

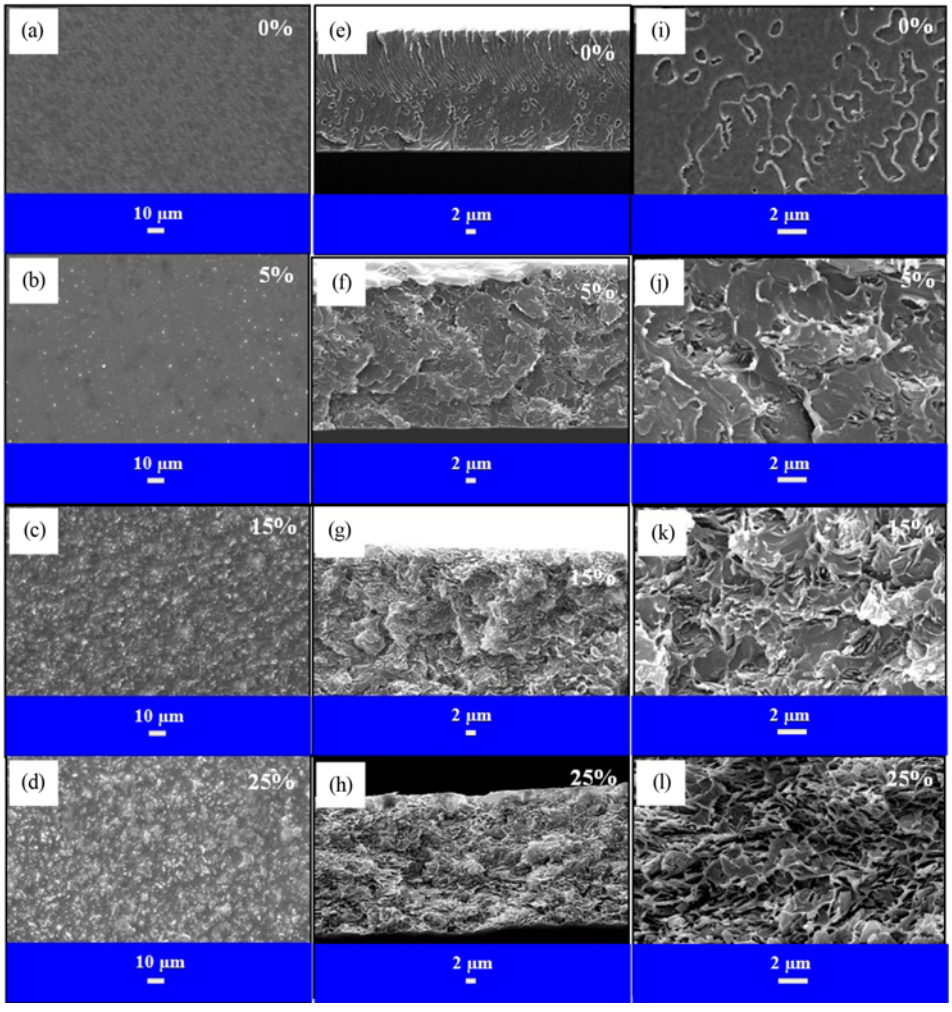

Fig. 6. SEM images of the 0, 5, 15, and 25% T-MOF-5/PEI MMMs.

in the production of ZnO [22]. In contrast, no extra ZnO molecule was present in C-MOF-5 structure because H_2O_2 was not employed in the synthesis [22,29].

Nitrogen adsorption experiments performed on T-MOF-5 nanocrystals were at 77 K and shown in Fig. 3. The BET surface area of T-MOF-5 was found to be 1,280 m^2/g and is lower from C-MOF-5 [29]. The lower BET surface of T-MOF-5 than C-MOF-5 is attributed to ZnO molecule [22].

The pore size distribution of the T-MOF-5, mainly 6.3 Å, was determined using the SHN1 method, as shown in Fig. 4. The textural property of T-MOF-5 is summarized in Table 1.

SEM image shows that the average particle size of T-MOF-5 nanocrystals was 90 nm (Fig. 5) with no defined morphology. Similar SEM images were obtained by another research group [3].

2. T-MOF-5/PEI Mixed-matrix Membranes

2-1. Membrane Characterization

The morphology strongly affects the transport properties in T-MOF-5/PEI MMMs. The morphology of the prepared pure PEI and T-MOF-5/PEI MMMs was investigated using scanning electron microscopy (SEM). Fig. 6 shows the surface ((a), (b), (c) and (d)) and cross-section at low magnification ((e), (f), (g) and (h)) and high magnification ((i), (j), (k) and (l)) of 0, 5, 15, and 25% (w/w) T-MOF-5/PEI MMMs.

In cross-section SEM images, many T-MOF-5 can be observed. These images indicate that the filler particle distribution is good enough due to ultra sonic homogenization. As shown in Fig. 6, the membrane morphology changed with T-MOF-5 nanocrystal loading. In other words, the pure PEI membrane shows a dense morphology with no plastic deformation and the T-MOF-5/PEI MMMs cross-section morphology reveals the formation of polymer veins and pores with increased plastic deformation of the pure PEI membrane [3].

It can be observed that there is little agglomeration of T-MOF-5 along the T-MOF-5/PEI MMMs preparation. In addition, from the cross-sections SEM images, there are little non-selective voids between PEI phase and T-MOF-5 particles along the MMMs. According to obtained results (with no surface modifying agent), it can be claimed that the T-MOF-5/PEI contact is acceptable as also is approved by the gas permeation measurements. Similar results for C-MOF-5/PEI MMMs are reported by Arjmandi and Pakizeh [29].

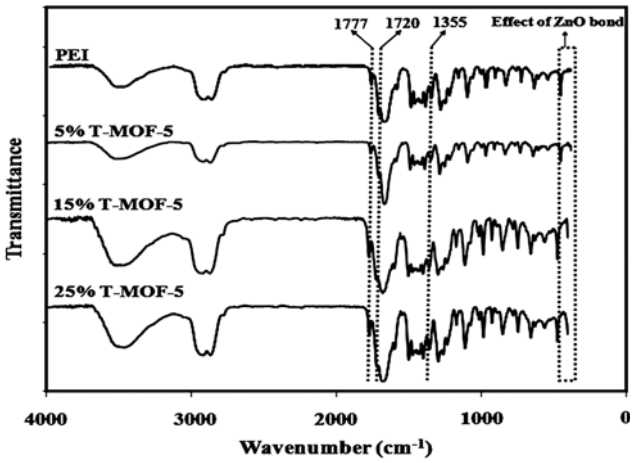

Fig. 7. The FTIR spectra of PEI and T-MOF-5/PEI MMMs.

The FTIR spectra of pure PEI and T-MOF-5/PEI hybrid membranes are depicted in Fig. 7. The absorption bands at 1,777, 1,720 cm^{-1} (asymmetric and symmetric C=O stretching vibration), 1,355 cm^{-1} (C-N stretching, phthalimide rings) [41,42] and also vibrations at 1,268, 1,234, 1,072, and 1,014 cm^{-1} (resulting from aryl ether bonds) [43] are observed in all nanocomposite membranes. According to the presence of benzene rings in PEI and T-MOF-5, there is an increased peak intensity in the range of 530-4,000 cm^{-1} and a slight shift in peak frequencies. In other Thus, due to similar chemical bonds, relative overlapping between the bands of the T-MOF-5 and PEI is observed. A similar result was reported by Arjmandi and Pakizeh [29] in C-MOF-5/PEI MMMs FTIR studies. In the spectrum of the 400-530 cm^{-1} that is characteristic of ZnO molecules [23,38,40], we can observe that, by increasing the percentage of T-MOF-5 loading, the absorption band of symmetric Zn=O appears with high intensity.

Table 2. Gas permeabilities (Barrer) of various gases through the pure PEI and T-MOF-5/PEI MMMs at 25 °C and 6 bar

Polymer	T-MOF-5 in polymer (W/W)	H_2	CO_2	CH_4	N_2
PEI	0	10.1±1	1.7±0.2	0.09±0.02	0.10±0.02
	5	13.2±1	1.9±0.1	0.10±0.02	0.11±0.02
	15	17±1	2.1±0.1	0.11±0.03	0.13±0.02
	25	25.2±1	3±0.3	0.12±0.01	0.14±0.01

Table 3. Diffusivity ($\times 10^{-8}$ cm^2/s) and solubility ($\times 10^{-2}$ cm^3 (STP)/cm cmHg) coefficients of the CO_2, CH_4 and N_2 in pure PEI and T-MOF-5/PEI MMMs at 25 °C and 6 bar

Polymer	T-MOF-5 in polymer (W/W)	Diffusivity coefficient			Solubility coefficient		
		CO_2	CH_4	N_2	CO_2	CH_4	N_2
PEI	0	0.15	0.090	0.11	11.01	1	0.9
	5	0.16	0.094	0.12	12.2	1.1	0.92
	15	0.17	0.098	0.14	12.87	1.13	0.93
	25	0.19	0.104	0.15	15.46	1.27	0.94

2-2. Gas Permeation

Table 2 shows H_2, CO_2, CH_4 and N_2 permeability results of pure PEI and T-MOF-5/PEI MMMs at varying mass fraction (w_d) of T-MOF-5 nanocrystals. These results were obtained by averaging values from three replicate permeation tests over each membrane at 25 °C and 6 bar upstream pressure.

From Table 2, all gases' permeability was increased with T-MOF-5 loading. As can be elucidated from Table 2, the permeability of all gases in pure PEI and T-MOF-5/PEI MMMs membrane varies in the following order:

$H_2>CO_2>N_2>CH_4$

The results obtained for H_2 show that an increase in permeability from 10.07 barrer to 25.17 barrer in T-MOF-5/PEI MMMs was achieved, suggesting that the T-MOF-5 nanocrystals were facilitating gas transport through the membrane (Table 2).

The differences observed in the permeability results of the membranes can be explained through the solution-diffusion mechanism [44]. The differences in permeability can be better realized by studying the contributions of diffusivity (D) and solubility (S) coefficients in permeability. The diffusivity of the gases (except H_2) was measured according to the time lag method using Eq. (3). The solubility of the gases for each sample was then calculated according to Eq. (4) using the permeability and diffusivity values of the gases.

Table 3 summarizes the diffusivity and solubility values of the CH_4, N_2 and CO_2 for the PEI and T-MOF-5/PEI MMMs at different weight fractions of T-MOF-5 nanocrystals.

As can be seen in Table 3, incorporating of T-MOF-5 in polymer phase as filler leads to increase in diffusivity and solubility coefficients and finally the gas permeability.

Fig. 8 shows the relative permeability, diffusivity and solubility of the N_2, CH_4 and CO_2 in T-MOF-/PEI (this study) and C-MOF-5/PEI [29] MMMs as a function of T-MOF-5 and C-MOF-5 loading. Also, Fig. 9 represents the relative permeability (P_r) of H_2.

As noted earlier, the T-MOF-5 has lower surface area, lower porosity, smaller and more uniform pore size, and more ZnO molecule than C-MOF-5. The differences between the T-MOF-5 and C-MOF-5 bring about the different behaviors as filler in MMMs.

As can be observed in Figs. 8 and 9, the relative permeability of all gases was increased for both T-MOF-5/PEI and C-MOF-5/PEI MMMs. The results show that for all gases (except H_2) the order of the relative permeability in the C-MOF-5/PEI MMMs is much greater than order of T-MOF-5/PEI MMMs. In the case of H_2, the order of the relative permeability in the T-MOF-5/PEI MMMs is approximately similar to the order of C-MOF-5/PEI MMMs (see Figs. 8 and 9).

In Fig. 8, the relative diffusivity of CO_2, N_2, and CH_4 increased with tetragonal and cubic MOF-5 loading. The increase in diffu-

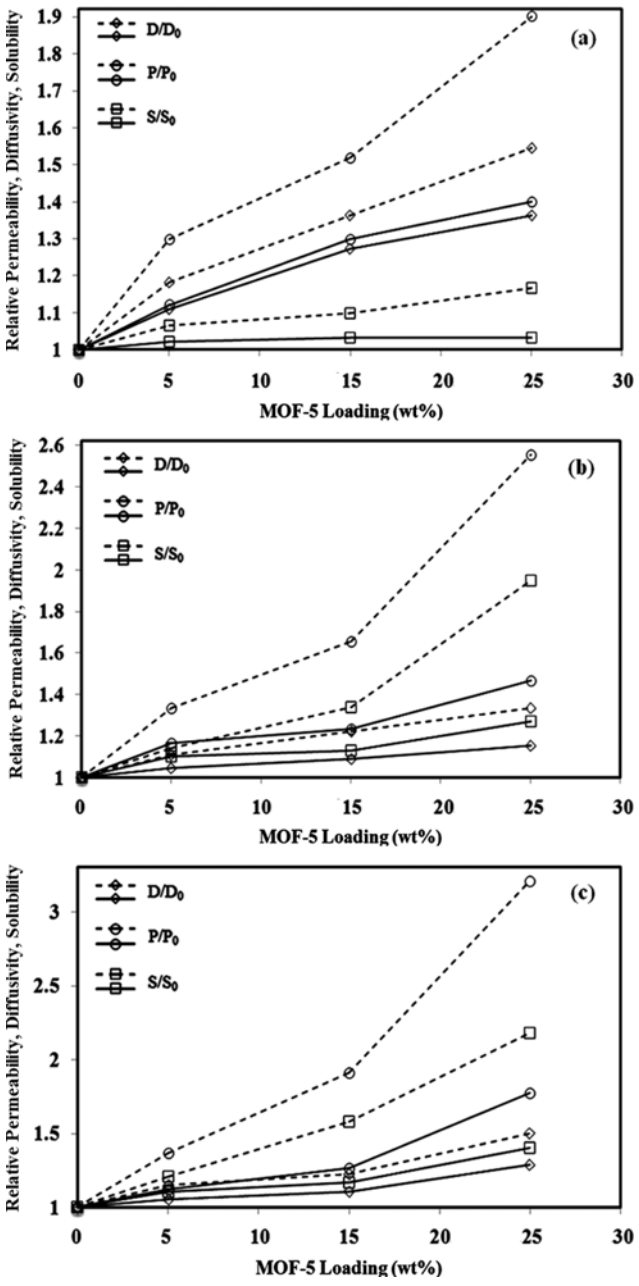

Fig. 8. Enhancement of gas transport properties for (a) N_2, (b) CH_4 and (c) CO_2 in T-MOF-5/PEI (continuous line) and C-MOF-5/PEI [29] (discontinuous line) MMMs as a function of MOF-5 loading.

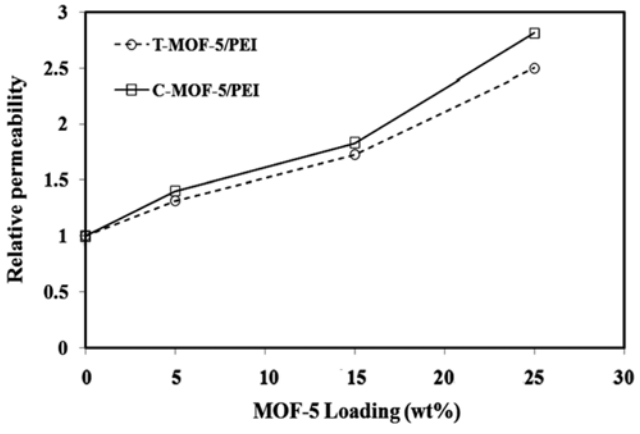

Fig. 9. H_2 relative permeability in T-MOF-5/PEI (continuous line) and C-MOF-5/PEI [29] (discontinuous line) MMMs as a function of MOF-5 loading.

Table 4. Pure gas ideal selectivity for pure PEI and T-MOF-5/PEI MMMs at 25 °C and 6 bar

Polymer	T-MOF-5 in polymer (W/W)	$\alpha^{p}_{i,j}=P_i/P_j$				$\alpha^{D}_{i,j}=D_i/D_j$		$\alpha^{S}_{i,j}=S_i/S_j$	
		$\alpha^{p}_{H_2,\,CO_2}$	$\alpha^{p}_{H_2,\,CH_4}$	$\alpha^{p}_{CO_2,\,CH_4}$	$\alpha^{p}_{CH_4,\,N_2}$	$\alpha^{D}_{CO_2,\,CH_4}$	$\alpha^{D}_{CH_4,\,N_2}$	$\alpha^{D}_{CO_2,\,CH_4}$	$\alpha^{D}_{CH_4,\,N_2}$
PEI	0%	5.99	111.89	18.67	0.9	1.67	0.82	11.01	1.11
	5%	6.99	125.9	18	0.94	1.68	0.77	11.1	1.19
	15%	8	153.51	19.19	0.85	1.69	0.7	11.39	1.21
	25%	8.45	208.02	22.57	0.94	1.86	0.69	12.17	1.36

sivity coefficient is dependent on the porosity introduced by the tetragonal (pore size 6.3 Å) and cubic (pore size 8.67 Å) MOF-5. Moreover, the pore size of both MOF-5s is greater than the molecular diameters of all gases tested. When the pore size is reduced from 8.67 Å (C-MOF-5) to 6.3 Å (T-MOF-5), then it can be expected that the diffusivity coefficient of largest and smallest gas undergoes the most and least reduction.

Additionally, the results presented in Fig. 8 show that the gas solubility of CO_2, N_2, and CH_4 increased with both MOF-5s loading. According to the results of Sholl's simulated adsorption isotherms of CO_2, N_2, and CH_4 in MOF-5 adsorbent [28] and C-MOF-5/PEI MMMs [29], it can be said that after incorporation of C-MOF-5 nanocrystals into the PEI, for N_2, the solubility remained relatively unchanged. But, because CO_2 has a strong affinity toward MOF-5, the CO_2 solubility has been particularly increased. Also, similar behavior about CH_4 solubility has also been observed, but the order of increase in CO_2 solubility is greater than the CH_4 solubility. According to our results, similar behavior has been observed by the T-MOF-5/PEI MMMs. As mentioned earlier, the T-MOF-5 contains less CO_2 and benzene (organic ligand) molecule versus T-MOF-5. Considering that the organic ligand in MOF-5 structure is the major site of adsorption of CO_2 and CH_4 [26], it can be expected that CO_2 solubility in T-MOF-5/PEI MMMs is less than that in C-MOF-5/PEI MMMs. As can be observed in Fig. 8, the relative solubility of CO_2 gas through the T-MOF-5/PEI MMMs significantly increases in comparison with the C-MOF-5/PEI MMMs. However, the increased permeability of the condensable CO_2 and CH_4 gases is mainly related to the enhancement of gas solubility due to increasing of the active sites for gas solution in polymer matrix. The comparison of the relative solubility of the CO_2 gas under study in 25%T-MOF-5/PEI and 25%C-MOF-5/PEI composite membranes indicates an increase in the solubility of 1.41 and 2.17 times, respectively.

According to Fig. 8, it can be concluded that for both MOF-5s the relative permeability of the CO_2 and CH_4 is strongly affected by the solubility coefficient and less affected by the diffusion coefficient. The relative permeability of N_2 is more affected by the diffusion coefficient than solubility coefficient.

In the case of H_2 the solubility and diffusivity coefficients were not calculated in this study due to its high response, but according to Sholl's results about H_2 diffusion coefficient inside C-MOF-5 pores, it seems likely that the H_2 permeability is enhanced by the diffusivity and not by the solubility [28,29]. Because the kinetic diameter of hydrogen is very small, then it can be expected that changing the pores size from cubic (8.67 Å) to tetragonal (6.3 Å) has little effect on the H_2 diffusivity. Also as mentioned earlier, the inorganic cluster is the major site of H_2 adsorption in MOF-5 (containing ZnO molecule). Given that the T-MOF-5 versus C-MOF-5 has more ZnO molecules, then the site of H_2 adsorption in T-MOF-5 is more than that in C-MOF-5. Accordingly, it can be expected that H_2 solubility in T-MOF-5/PEI MMMs is more than that in C-MOF-5/PEI MMMs. Considering the speculations about diffusivity and solubility of membranes containing T-MOF-5 and C-MOF-5, it can be said that with changing the filler structure from cubic to tetragonal, we will see the lowest permeability drop for H_2. This situation can be clearly seen in Fig. 9.

Ideal selectivity based on permeability (permselectivity) ($\alpha^{p}_{i,j}$), diffusivity ($\alpha^{D}_{i,j}$) and solubility ($\alpha^{S}_{i,j}$) in T-MOF-/PEI MMMs as a function of T-MOF-5 loading at 25 °C and 6 bar for H_2/CO_2, H_2/CH_4, CO_2/CH_4 and CH_4/N_2 are presented in Table 4.

As shown in Table 4, for the 5 wt% T-MOF-5 in PEI, the permselectivity ($\alpha^{p}_{i,j}$) values for H_2/CO_2, H_2/CH_4 and CO_2/CH_4 were increased with T-MOF-5 loading (for example, around 17% for H_2/CO_2 T-MOF-5/PEI MMMs) and for 15 and 25 wt% T-MOF-5 loading, the permselectivity of H_2/CO_2 increased around 34 and 42%, respectively. Reverse results were reported for H_2/CO_2 in C-MOF-5/PEI by Arjmandi and Pakizeh [29]. As mentioned earlier, with changing the structure from cubic to tetragonal, H_2 gas will undergo the lowest permeability drop. Because the adsorption site of CO_2 in T-MOF-5 is less than that in C-MOF-5 and also the adsorption site of H_2 in T-MOF-5 is more than that in C-MOF-5, then we can attribute the H_2/CO_2 permselectivity increase to three factors: 1) very low decreasing the relative permeability of H_2 in T-MOF-5/PEI MMMs compared to C-MOF-5/PEI MMMs; 2) decreasing the CO_2 adsorption site with changing structure from cubic to tetragonal; and 3) increasing the H_2 adsorption site with changing structure from cubic to tetragonal.

Except for H_2/CO_2, the H_2/CH_4, CO_2/CH_4 and CH_4/N_2 permselectivity in T-MOF-5/PEI MMMs increased further.

2-3. Modeling of Gas Permeability in MMMs

The permeability behavior of T-MOF-5/PEI MMMs has been modeled using the Higuchi model [45]. This model can be approximately simplified to:

$$P_{eff}=P_c+\frac{3\varnothing_d P_c}{[1-\varnothing_d+K(1-\varnothing_d)]} \quad (5)$$

where, P_{eff} is the overall permeability of the MMM, P_c is continuous phase permeability and $\varnothing_d$ is volume fraction of filler in the MMM. The Higuchi constant, K, is an empirical constant that was selected to be 0.78 by Higuchi for the best fit of the experimental data to model [45]. In our previous work we tried to fit the Higuchi model for estimation of the gas permeability of C-MOF-5/PEI

Table 5. The best K and R^2 value for different gases in the T-MOF-5/PEI MMMs at 25 °C and 6 bar

Parameter	H_2	CO_2	CH_4	N_2
K	0.77	0.53	0.12	0.25
R^2	0.99	0.95	0.8	0.91

MMMs [29] and found that there was no good compatibility between model and all experimental results supposing exactly K=0.78 in the Higuchi model. As reported in C-MOF-5/PEI MMMs [29], the Higuchi constant should change to be able to fit the Higuchi model to the experimental data. In the case of T-MOF-5/PEI MMMs, the Higuchi model by using a least square method was fitted to experimental data and the best K constants were derived for all gases. The obtained results for the best K and R^2 value for each of gases are listed in Table 5.

Fig. 10 also shows the experimental data and predicted data obtained from the Higuchi model applying K parameter from Table 5.

Regarding the data presented in Table 5, the order of the K parameter is in good agreement with the order of relative gases' permeability through the MMMs (P_r). The relative permeability (P_r) of all gases in the T-MOF-5/PEI MMMs was obtained as the following order:

$$P_r^{H_2}>P_r^{CO_2}>P_r^{N_2}>P_r^{CH_4}$$

Thus, the K parameter, which is closely related to the value of P_r, has the following order:

$$K_{H_2}>K_{CO_2}>K_{N_2}>K_{CH_4}$$

As a result, it can be concluded that by incorporation of T-MOF-5 in pure PEI, the K parameter will be changed. Fig. 10 shows that the Higuchi model can estimate the permeability of all gases in T-MOF-5/PEI MMMs, if the K values in this model are used correctly according to values presented in Table 5.

2-4. Evaluation of Gas Permeation Performance

Fig. 11 shows Robeson's upper bond trade-off line relationship between the H_2 permeability and the H_2/CO_2 (a) and H_2/CH_4 (b) selectivity for the T-MOF-5/PEI MMMs with the C-MOF-5/PEI MMMs [29] data at around 25 °C.

Also, based on the present results, the trade-off line relationship between the CO_2 permeability and the CO_2/CH_4 selectivity for T-MOF-5/PEI MMMs compared to C-MOF-5/PEI MMMs [29] was evaluated and presented in Fig. 12.

In Figs. 11 and 12, the incorporation of both tetragonal and cubic MOF-5 in pure PEI membrane increases the gas separation ability of MMMs for H_2/CO_2, H_2/CH_4 and CO_2/CH_4 separation, which means prepared MMMs present better separation performance than pure PEI membrane.

To separate H_2/CO_2 and H_2/CH_4, the C-MOF-5/PEI MMMs prepared in our previous work [29] reside close to the Robeson upper

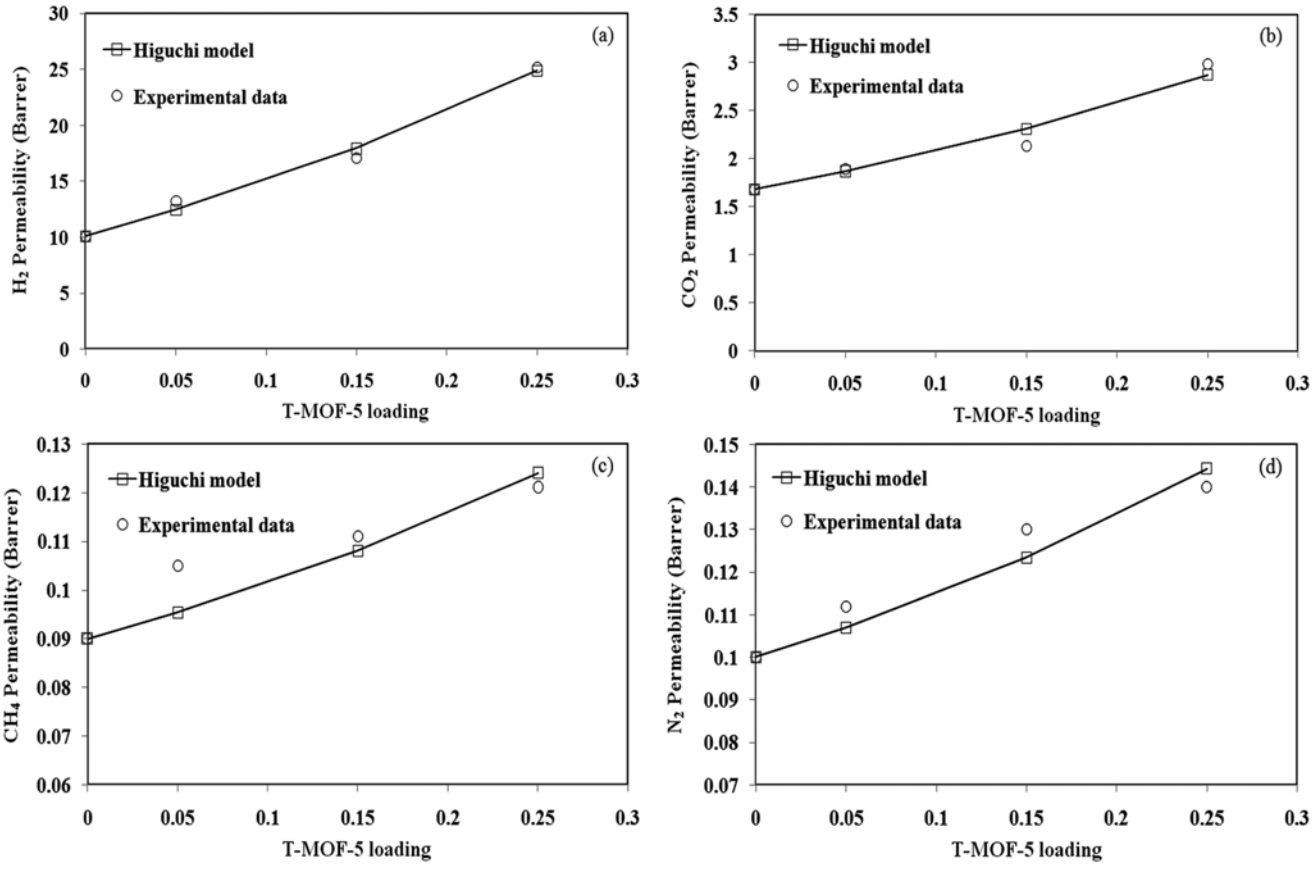

Fig. 10. Estimation of permeability coefficient to Higuchi model for (a) H_2, (b) CO_2, (c) CH_4 and (d) N_2 in T-MOF-5/PEI MMMs by considering new K value.

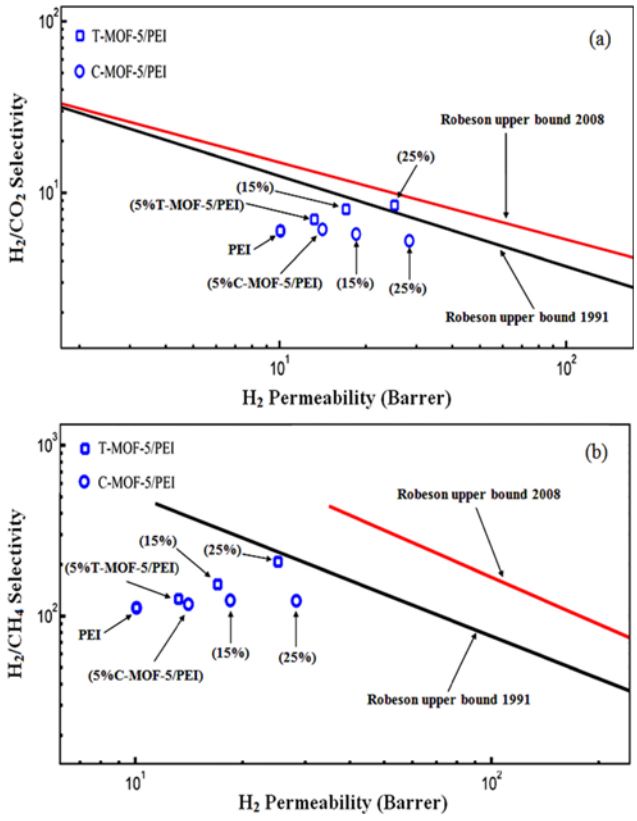

Fig. 11. (a) H_2/CO_2 and (b) H_2/CH_4 separation performance of PEI, T-MOF-5/PEI and C-MOF-5/PEI [29] MMMs in comparison to Robeson's upper line.

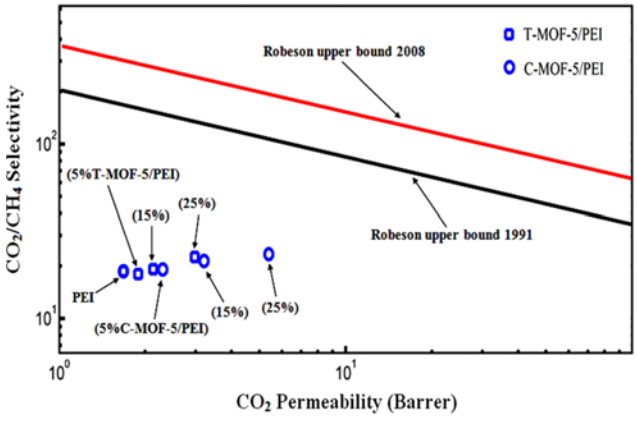

Fig. 12. CO_2/CH_4 separation performance of PEI, T-MOF-5/PEI and C-MOF-5/PEI [29] MMMs in comparison to Robeson's upper line.

bound, and the T-MOF-5/PEI MMMs prepared in this research reside above or close to the Robeson upper bound (as shown in Fig. 11). Also according to Fig. 12, as a result of the increased CO_2 solubility, the C-MOF-5/PEI MMMs present better CO_2/CH_4 separation performance than T-MOF-5/PEI MMMs.

A membrane with high permeability and good selectivity is indeed more industrially attractive. Therefore, tetragonal and cubic MOF-5s appear to be proper candidates for MMMs fabrication due to desirable increase perm-selectivity in H_2 and CO_2, respectively (compared to neat PEI membrane).

According to results, the C-MOF-5 nanocrystals as filler for MMMs have potential to enhance CO_2/CH_4 separation. And based on the results presented in this research the T-MOF-5 nanocrystals have potential to enhance H_2 separation from CO_2 and CH_4 (H_2/CO_2 and H_2/CH_4).

CONCLUSIONS

There are two types of MOF-5: one occupying the cubic structure and another the tetragonal. The T-MOF-5 had lower surface area, lower porosity, smaller and more uniform pore size, and more ZnO crystal than C-MOF-5. Also, according to thermogravimetric analysis the C-MOF-5 is more stable than the T-MOF-5. The tetragonal and cubic MOF-5s and novel MMMs containing T-MOF-5 inside a PEI were successfully prepared and characterized in this work and compared with C-MOF5-/PEI MMMs at varying mass fraction (w_d) of MOF-5 nanocrystals. The obtained results showed that the presence of more ZnO crystal in the T-MOF-5 structure could lead to decreasing the permeability at different levels (for all gases tested) while increasing the selectivity (for H_2/CO_2, H_2/CH_4 and CO_2/CH_4). SEM images of the MMMs show that by increasing the T-MOF-5 content in PEI, plastic deformation of the polymer occurred. According to the present results, the H_2, CO_2, CH_4 and N_2 permeability, diffusivity and solubility were increased at different levels with T-MOF-5 loading. Also, by incorporation of T-MOF-5 content in PEI the ideal selectivity ($\alpha^p_{i,j}$) of H_2/CO_2, H_2/CH_4 and CO_2/CH_4 were increased (at low and high loading of filler). CO_2 and CH_4 permeability and also N_2 permeability are strongly affected by the solubility and diffusivity coefficient, respectively. Considering the speculations about diffusivity and solubility of membranes containing T-MOF-5 and C-MOF-5, with changing the filler structure from cubic to tetragonal, we will see the lowest permeability drop for H_2. The permeations of H_2, CO_2, N_2 and CH_4 through T-MOF-5/PEI MMMs were fitted on Higuchi model and the new adjustable k value for Higuchi model was selected. The incorporation of T-MOF-5 in the PEI, can lead to an overall improvement in performance of permselectivity in relation to the Robeson upper line. In other words, the T-MOF-5 nanocrystals have potential to enhance H_2 separation from CO_2 and CH_4 (H_2/CO_2 and H_2/CH_4).

ACKNOWLEDGEMENTS

The authors acknowledge Iran Nanotechnology Initiative Council for financial support.

REFERENCES

1. S. Kim, L. Chen, J. K. Johnson and E. Marand, *J. Membr. Sci.*, **294**, 147 (2007).
2. H. B. Tanh Jeazet, C. Staudt and Ch. Janiak, *Dalton Trans.*, **41**, 13991 (2012).
3. E. V. Perez, K. J. Balkus Jr., J. P. Ferraris and I. H. Musselman, *J. Membr. Sci.*, **328**, 165 (2009).
4. W. J. Koros and R. Mahajan, *J. Membr. Sci.*, **175**, 181 (2000).

5. W. J. Koros and R. Mahajan, *Polym. Eng. Sci.*, **42**, 1420 (2002).
6. W. J. Koros and R. Mahajan, *Polym. Eng. Sci.*, **42**, 1432 (2002).
7. R. Mahajan and W. J. Koros, *Ind. Eng. Chem. Res.*, **39**, 2692 (2000).
8. S. Kulprathipanja, R. W. Neuzil and N. N. Li, US Patent, 4,740,219 (1988).
9. J.-M. Duval, B. Folkers, M. H. V. Mulder, G. Desgrandchamps and C. A. Smolders, *J. Membr. Sci.*, **80**, 189 (1993).
10. J.-M. Duval, A. J. B. Kemperman, B. Folkers, M. H. V. Mulder, G. Desgrandchamps and C. A. Smolders, *J. Appl. Polym. Sci.*, **54**, 409 (1994).
11. M. G. Suer, N. Bac and L. Yilmaz, *J. Membr. Sci.*, **91**, 77 (1994).
12. B. Zornoza, C. Tellez, J. Coronas, J. Gascon and F. Kapteijn, *Micropor. Mesopor. Mater.*, **166**, 67 (2013).
13. K. Hunger, N. Schmeling, H. B. Tanh Jeazet, Ch. Janiak, C. Staudt and K. Kleinermanns, *Membranes*, **2**(4), 727 (2012).
14. H. B. Tanh Jeazet, C. Staudt and Ch. Janiak, *Chem. Commun.*, **2140-2142**, 48 (2012).
15. H. B. Tanh Jeazet, T. Koschine, C. Staudt, K. Raetzke and Ch. Janiak, *Membranes*, **3**(4), 331 (2013).
16. O. G. Nik, X. Y. Chen and S. Kaliaguine, *J. Membr. Sci.*, **413-414**, 48 (2012).
17. O. M. Yaghi, G. Li and H. Li, *Nature*, **378**, 703 (1995).
18. S. Kitagawa, R. Kitaura and S. Noro, *Angew. Chem. Int. Ed.*, **43**, 2334 (2004).
19. U. Mueller, M. Schubert, F. Teich, H. Puetter, K. Schierle-Arndt and J. Pastre, *J. Mater. Chem.*, **16**, 626 (2006).
20. S. Bureekaew, S. Shimomura and S. Kitagawa, *Sci. Technol. Adv. Mater.*, **9**, 1 (2008).
21. H. Li, M. Eddaoudi, M. O'Keeffe and O. M. Yaghi, *Nature*, **402**, 276 (1999).
22. L. Zhang and Y. H. Hu, *Mater. Sci. Eng. B*, **176**, 573 (2011).
23. L. Huang, H. Wang, J. Chen, Z. Wang, J. Sun, D. Zhao and Y. Yan, *Micropor. Mesopor. Mater.*, **58**, 105 (2003).
24. S. S. Kaye, A. Dailly, O. M. Yaghi and J. R. Long, *J. Am. Chem. Soc.*, **129**, 14176 (2007).
25. M. Arjmandi and M. Pakizeh, *Act. Metal. Sin. (English Letters)*, **26**, 597 (2013).
26. R. A. Sarmiento-Perez, L. M. Rodriguez-Albelo, A. Gomez, M. Autie-Perez, D. W. Lewis and A. R. Ruiz-Salvador, *Micopor. Mesopor. Mater.*, **163**, 186 (2012).
27. E. C. Spencer, J. A. K. Howard, G. J. McIntyre, J. L. C. Rowsell and O. M. Yaghi, *Chem. Commun. (Camb)*, 278 (2006).
28. A. I. Skoulidas and D. S. Sholl, *J. Phys. Chem. B*, **109**, 15760 (2005).
29. M. Arjmandi and M. Pakizeh, *J. Ind. Eng. Chem.*, **20**, 3857 (2014).
30. G. Clarizia, C. Algieri, A. Regina and E. Drioli, *Micropor. Mesopor. Mater.*, **115**, 67 (2008).
31. S. Brunauer, P. H. Emmett and E. Teller, *J. Am. Chem. Soc.*, **60**, 309 (1938).
32. A. Shahsavand and M. Niknam Shahrak, *Colloids Surf., A*, **378**, 1 (2011).
33. M. A. Semsarzadeh, M. Sadeghi, M. Barikani and H Moadel, *Iran Polym. J.*, **16**, 819 (2007).
34. M. Sadeghi, M. A. Semsarzadeh, M. Barikani and B. Ghalei, *J. Membr. Sci.*, **354**, 40 (2010).
35. P. Galiatsatou, N. K. Kanellopoulos and J. H. Petropoulos, *J. Membr. Sci.*, **280**, 634 (2006).
36. W. J. Koros, D. R. Paul and A. A. Rocha, *J. Polym. Sci. Part B*, **14**, 687 (1976).
37. J. Hafizovic, M. Bjorgen, U. Olsbye, P. D. C. Dietzel, S. Bordiga, C. Prestipino, C. Lamberti and K. P. Lillerud, *J. Am. Chem. Soc.*, **129**, 3612 (2007).
38. R. Sabouni, H. Kazemian and S. Rohani, *Chem. Eng. J.*, **165**, 966 (2010).
39. N. T. S. Phan, K. K. A. Le and T. D. Phan, *Appl. Cat. A*, **382**, 246 (2010).
40. J. Coates, *Interpretation of infrared spectra, a practical approach,* Wiley, New York (2000).
41. W. Albrecht, B. Seifert, T. Weigel, M. Schossig, A. Hollnder, T. Groth and R. Hilke, *Macromol. Chem. Phys.*, **204**, 510 (2003).
42. A. I. Romero, M. L. Parentis, A. C. Habert and E. E. Gonzo, *J. Mater. Sci.*, **46**, 4701 (2011).
43. S. T. Amancio-Filho, J. Roeder, S. P. Nunes, J. F. dos Santos and F. Beckmann, *Polym. Degrad. Stab.*, **93**, 1529 (2008).
44. R. Kesting and A. K. Fritzsche, *Polymeric gas separation membranes,* Wiley, New York (1993).
45. W. I. Higuchi, *J. Phys. Chem.*, **62**, 649 (1958).